Osteoarthritis and Cartilage

OARSI OSTEOARTHRITIS RESEARCH SOCIETY INTERNATIONAL

Phase-contrast enhanced synchrotron micro-tomography of human meniscus tissue

E. Einarsson † ‡ * a, M. Pierantoni § a, V. Novak ¦, J. Svensson † ¶, H. Isaksson §, M. Englund ‡

† *Medical Radiation Physics, Department of Translational Medicine, Lund University, Malmö, Sweden*
‡ *Clinical Epidemiology Unit, Orthopedics, Department of Clinical Sciences Lund, Lund University, Lund, Sweden*
§ *Department of Biomedical Engineering, Lund University, Lund, Sweden*
¦ *Swiss Light Source, Paul Scherrer Institute, Villigen, Switzerland*
¶ *Medical Imaging and Physiology, Skåne University Hospital, Lund, Sweden*

ARTICLE INFO

SUMMARY

Objective: To investigate the feasibility of synchrotron radiation-based phase contrast enhanced micro-computed tomography (SR-PhC-μCT) for imaging of human meniscus. Quantitative parameters related to fiber orientation and crimping were evaluated as potential markers of tissue degeneration.

Design: Human meniscus specimens from 10 deceased donors were prepared using different preparation schemes: fresh frozen and thawed before imaging or fixed and paraffin-embedded. The samples were imaged using SR-PhC-μCT with an isotropic voxel size of 1.625 μm. Image quality was evaluated by visual inspection and spatial resolution. Fiber voxels were defined using a grey level threshold and a structure tensor analysis was applied to estimate collagen fiber orientation. The area at half maximum (FAHM) was calculated from angle histograms to quantify orientation distribution. Crimping period was calculated from the power spectrum of image profiles of crimped fibers. Parameters were compared to degenerative stage as evaluated by Pauli histopathological scoring.

Results: Image quality was similar between frozen and embedded samples and spatial resolutions ranged from 5.1 to 5.8 μm. Fiber structure, including crimping, was clearly visible in the images. Fibers appeared to be less organized closer to the tip of the meniscus. Fiber density might decrease slightly with degeneration. FAHM and crimping period did not show any clear association with histopathological scoring.

Conclusion: SR-PhC-μCT is a feasible technique for high-resolution 3D imaging of fresh frozen meniscus tissue. Further work is needed to establish quantitative parameters that relate to tissue degeneration, but this imaging technique is promising for future studies of meniscus structure and biomechanical response.

Introduction

The menisci are of great importance for the function of the knee joint as they distribute load and reduce the pressure on the articular cartilage. Although not yet fully understood, meniscus degeneration is associated with the development of knee osteoarthritis (OA)[1]. Meniscus tissue consists mainly of collagen type I fibers forming bundles oriented in a circumferential pattern[2]. The fibers are crimped in a similar way as fibers in for example tendons and ligaments[3]. Crimping morphology has not been extensively studied in the meniscus[4,5] but is likely associated with mechanical properties, such as the ability to withstand tensile stress[6]. With degeneration, the collagen network is disrupted, and fibers are less organized[7,8]. To assess how the meniscus and its function is affected during OA development, methods to detect and follow these structural changes are required.

For non-invasive imaging of the meniscus *in vivo*, magnetic resonance imaging (MRI) is the preferred method. A disadvantage, however, is the limited spatial resolution of MRI, commonly in the order of tenths of a mm per voxel, in plane, and often even larger

* Address correspondence and reprint requests to: E. Einarsson, Medical Radiation Physics, Skane University Hospital Malmö, Carl-Bertil Laurells gata 9, 4th floor, 214 28 Malmö, Sweden.

E-mail address: emma.einarsson@med.lu.se (E. Einarsson).

a Equal contributions as first author.

slice thickness. Even though there exist quantitative MR-based techniques with the potential of probing the microscopic environment of the meniscus, the visualization of the tissue is limited to macroscopic structures[9]. For *ex vivo* imaging on the other hand, histology is considered the gold standard method for evaluation of tissue quality at a microscopic level but is limited to (2D) imaging of thin slices and relies on tissue preparation and staining. Microscopy techniques such as polarized light microscopy (PLM) or scanning electron microscopy (SEM) offers high resolution but are also destructive, limited to 2D and requires fixation of the tissue samples.

Micro computed tomography (μCT) enables 3D imaging with high resolution. Laboratory μCT is advantageous because of its availability but scan times are long and for low absorption materials and tissues, contrast agents are usually required. Using a synchrotron light source for μCT enables fast 3D imaging with (sub) micrometrical spatial resolution, due to the high flux and coherence of the beam[10,11]. It also offers the possibility to use phase contrast enhancement (PhC) which improves the soft tissue contrast without the use of contrast agents[9,12].

Synchrotron radiation-based phase contrast enhanced micro computed tomography (SR-PhC-μCT) has the potential of resolving individual fibers and fiber bundles and to directly visualize collagen organization in a 3D volume. This method also offers the possibility to image tissue samples without fixation or other preparation of the tissue[13] and may therefore be suitable for studies of meniscus biomechanics. SR-PhC-μCT has been performed with promising results in soft musculoskeletal tissues, e.g., intravertebral discs, articular cartilage, and tendon[10,11,13]. Horng *et al.* also performed CT with SR-PhC of entire human knee joints[9]. However, to the best of our knowledge, SR-PhC-μCT has not been evaluated for the study of microscopic collagen structure in meniscus tissue. For the potential use of this method in studies of meniscus biomechanics, it is also of interest to evaluate image quality with and without tissue fixation and embedding.

Since disorganization of the collagen structure is a characteristic of meniscus degeneration, quantification of fiber orientation is of great interest. Orientation analysis using structure tensors is a method that was originally developed for investigation of fiber structures in material science[14,15]. It has been adopted for use in medical science in images of highly structured tissues such as tendon and meniscus[16,17]. Measurements of crimping period, frequency and angle has been reported to describe the response to mechanical load of meniscus tissue[18—20]. Combining these types of image analysis with high resolution synchrotron imaging may prove valuable for evaluation of degenerative processes in the meniscus at a microscopic level.

Our aim with this study was to investigate the feasibility of SR-PhC-μCT in meniscus tissue to visualize the collagen structure and to evaluate the effect of sample preparation on the image quality. Further, we aimed to explore if crimping pattern characterization and orientation analysis of such images could be used to describe degeneration of meniscus tissue.

Methods

In brief, human meniscus samples were imaged using SR-PhC-μCT. The images were evaluated visually as well as quantitatively and comparisons were performed between sample preparations, between the different zones of the menisci and to histopathological scoring. The study was approved by the ethics committee at Lund University (Dnr 2015—39, 2016-865, and 2019-00323). Each step of the methods used are described in detail in the following sections.

Tissue samples

We used human menisci from a local biobank at Skåne University Hospital where the specimens were fresh frozen and stored at $-80°C$. Ten medial and six lateral menisci sampled from 10 deceased donors (i.e., both medial and lateral menisci from six donors and only medial menisci from four donors), 18—77 years old, five men and five women. Donors were without known knee OA, but the menisci showed varying degree of degeneration as previously evaluated by histopathological scoring[21]. Both vertical and horizontal histology slices from the body/posterior horn were stained using hematoxylin and eosin and safranin-o fast green and histopathological scoring was performed according to the Pauli histopathological scoring system[7,21]. Total Pauli score for the menisci ranged from 5 to 17 out of 0—18.

The menisci were thawed and a 4 mm thick vertical slice was cut from the body of each meniscus, adjacent to the location of the histological slices [Fig. 1(a)]. The sample slices were glued to the inside of the lid of 0.5 ml Eppendorf tubes and stored in phosphate buffered saline (PBS) at $-20°C$ until imaging. From three of the menisci (of varying age and including both sexes) an additional slice was cut which was fixated in formalin (buffered 4% formalin solution, pH 7) for 48 h and embedded in paraffin.

Phase contrast enhanced tomographic imaging

The thawed meniscus samples were imaged using SR-PhC-μCT at the TOMCAT beamline at the Swiss Light Source (Paul Scherrer Institute, Switzerland)[22]. The setup was optimized as previously described for tendon tissue by Pierantoni *et al.*[13]. The images were acquired using the High Numerical Aperture Microscope setup (4× magnification, field of view of 4.2 mm × 3.5 mm and pixel size of 1.625 μm) coupled to a LuAG:Ce scintillator screen of 150 μm. Two sequential tomographic volumes were imaged for each sample, starting at the tip of the meniscus, and then moving the sample 3 mm down to image the next part of the sample [Fig. 1(b)—(d)]. 2001 projections were captured with a pco. edge 5.5 camera over 180° with 33 ms exposure time, beam energy of 15 keV, and propagation distance of 150 mm. All projections were corrected with dark and flat-field images. A Paganin phase retrieval was used to calculate the sample projected density[23] and reconstructions were performed as described in Marone *et al.*[24] with a ratio δ:β of 50:1 (where β is the absorption coefficient $= 9.3 \times 10^{-9}$ and δ is the refractive index decrement).

Image analysis

All image analysis were performed in MATLAB (version R2020a), while we used ImageJ (Fiji) for visual inspection.

The image volumes were acquired approximately as sagittal cross sections of the meniscus. Images were then rotated using the sample border as a guide so that circumferential fibers in the meniscus are seen as horizontally and in-plane oriented in the image stack. For illustration, the two image volumes from one sample were merged by removing the overlap from one of the volumes and concatenating the matrices [Fig. 1(e)]. Two volumes of interest (VOI) in each meniscus, each covering $0.5 \times 0.5 \times 0.5$ mm^3 were manually chosen approximately at the center of the inner zone (i.e., near the tip of the meniscus) and the center of the middle zone (i.e., the central part of the meniscus) respectively [Fig. 1(e) and (f)].

Spatial resolution

As a measure of image quality, spatial resolution was calculated and compared between the two sample preparations. Spatial
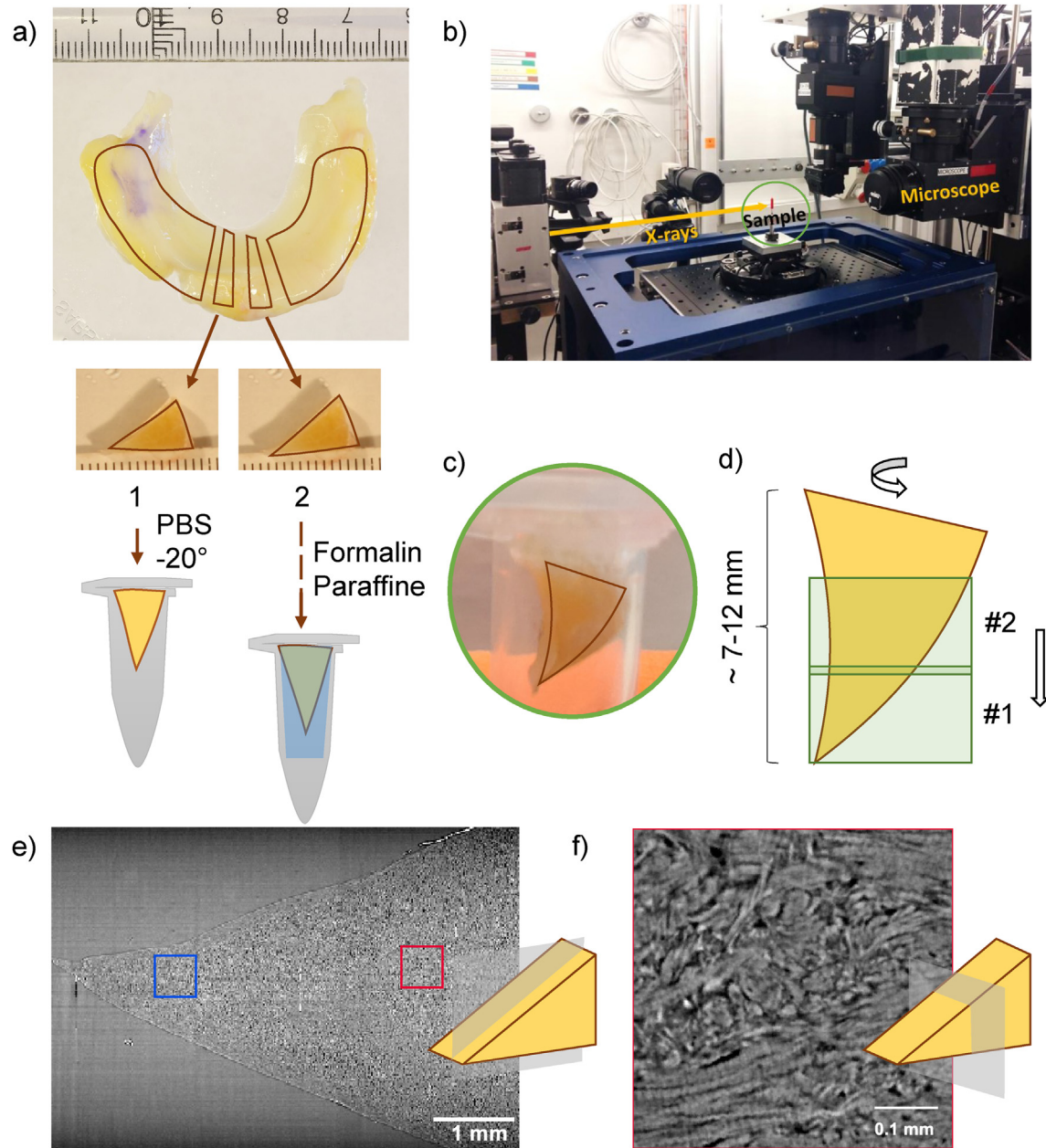
Fig. 1

Osteoarthritis and Cartilage

(a) Schematic representation of the dissection and preparation of two slices of a human meniscus. The first slice (all menisci) was frozen in PBS and the second (three menisci) was fixed in formalin and embedded in paraffin. (b) The SR-PhC-µCT imaging set-up at the TOMCAT beamline, Swiss Light Source. (c) Magnification of the sample positioned for imaging. (d) Schematic picture of the imaging procedure. The first acquisition covered the tip of the meniscus sample and after moving the sample 3 mm down a second image volume was acquired with a small overlap. (e) A reconstructed image from the two consecutive volumes stitched together and viewed in a coronal plane as illustrated by the schematic figure. Two small VOIs were placed, one at the tip (blue) and one in the central part of the meniscus (red). (f) Approximately sagittal oriented slice from the VOI positioned in the central part of the sample.

resolution was calculated in three orthogonal directions and averaged within a $0.5 \times 0.5 \times 0.5$ mm^3 VOI in the central part of the meniscus sample. The power spectrum was calculated by applying a fast Fourier transform to the data and spatial resolution was defined as the frequency where the intensity was two times the noise level, as suggested by Modregger *et al.*[25]. The noise level was defined as the value that the power spectrum converged to which was found by averaging the spectrum over the last third of the

frequencies[13,25,26]. Spatial resolution can be defined as the minimum distance at which two features can be resolved in the image[27]. Thus, it is for us a mean to determine the smallest structural characteristics that we can visualize and analyze. Furthermore, spatial resolution accounts for the characteristics of both the imaging system and of the samples (e.g., source and system stability, imaging artefacts) which cannot be fully determined a priori.

Thresholding

For the purpose of the orientation analysis described in the next section, a mask was created to only include fiber voxels. Pixel intensity of the images was normalized to grey values of 0–1. As fibers and surrounding tissue have different image intensity, fiber voxels can be separated from the background using thresholding of the normalized grey values. This was also used to determine the fiber density defined as: volume occupied by fibers/total volume, i.e., the percentage of the voxels within the VOI that was categorized as fibers. The threshold was set using Otsu's method which defines the threshold by minimizing the intensity variance between the different classes of pixels (in this case fibers and background)[28].

Orientation maps

Fiber orientation maps were generated using methods previously described by Mulat *et al.* and Krause *et al.*[14,29]. In short, the masked images were smoothed using a cubic kernel with a Gaussian distribution with a standard deviation of 2. A suitable level of smoothing was determined to reduce noise while still being able to capture fiber orientation (Fig. S1). Image gradients were found using a Sobel filter. Based on the gradients, a structure tensor was calculated voxel wise in the VOI. Gaussian smoothing was applied again, this time with a standard deviation of 0.5, on the resulting structure tensor. Eigenvectors and corresponding eigenvalues were calculated from the smoothed structure tensor, where the 3rd eigenvector, corresponding to the smallest eigenvalue, describes the fiber orientation. The orientation is presented in spherical coordinates using the azimuth and elevation angles.

For fiber voxels, the distribution of azimuth and elevation angles were evaluated together using combined histograms with 100×100 bins (Supplementary Fig. S2). The full area at half maximum (FAHM) of the combined histograms, in percentage of the total number of bins, were calculated as a measure of the spread in orientation, combining both the azimuth and elevation angles.

Crimp period

Crimping patterns could be identified in several locations in the middle zone of most of the menisci. In five locations per sample, avoiding artifacts, image profiles were manually drawn along crimped fibers, perpendicular to the crimps. Each profile was detrended using a polynomial function to remove contributions of larger fluctuations in intensity over the image (Supplementary Fig. S3). A fast Fourier transform was used to find the frequency (f) of the crimping pattern which was converted to crimp period (d) through $d = \frac{1}{f}$[18] and a mean value was calculated for each sample.

Statistical analysis

For the fiber density, FAHM and crimping period, we report mean values and standard deviations among the meniscus samples. Comparisons of parameters to Pauli score were performed using mixed effects linear models to compensate for the potential bias of medial and lateral menisci from the same individuals. The slope coefficient with 95 % confidence interval (CI) is presented as a measure of the association.

Results

Effect of sample preparation on image quality

Qualitative evaluation

For two of three paraffin embedded samples, image quality appeared fairly similar in visual comparison to the fresh frozen samples (Fig. 2). The collagen structure was clearly visible and crimping pattern could be seen in both type of samples. Images of the third paraffin embedded sample suggested some problems may have occurred during the sample preparation, and it was therefore excluded from further analysis (Supplementary Fig. S4).

Spatial resolution

Mean spatial resolution was similar in samples regardless of preparation procedure. For comparison, mean spatial resolution was 5.7 ± 0.7 and 5.4 ± 0.3 μm, respectively, in the two paraffin embedded samples. Corresponding values for the samples in PBS from the same two menisci were 5.8 ± 1.0 and 5.1 ± 0.1 μm.

Thresholding

Otsu's method resulted in similar number of voxels categorized as fibers in images from thawed samples in PBS and paraffin embedded samples with a mean difference of 7.3 percentage points. When plotting proportion of voxels categorized as fibers against the threshold, τ, it could be seen that contrast between fibers and background was higher for the paraffin embedded samples (Fig. 3).

Evaluation of tissue structure

Qualitative evaluation

The fibers were oriented, as expected, mainly in a circumferential order [Fig. 4(a)]. In general, fibers seemed to be more strictly organized in the middle zone compared to the inner zone [Fig. 4(e)]. Comparisons between degenerated and visibly intact tissue revealed clear structural differences with more loosely structured fibers, less crimping and larger cavities in between fibers (Fig. 5). These differences were more pronounced closer to the surface of the meniscus. Fig. 6 displays example orientations maps from a degenerated sample. Example videos of both normal and degenerated tissue can be found in the supplementary material.

Supplementary video related to this article can be found at https://doi.org/10.1016/j.joca.2022.06.003

Fiber density

The inner zone of one of the most degenerate samples (total Pauli score 14) was very frayed and the images suffered from artifacts. Because of the difficulty to place a VOI, this region was excluded from the quantitative evaluation.

The fiber density did not vary much between the different fresh frozen meniscus samples or between the inner and the middle zone in the respective sample [Fig. 7(a)]. In the middle zone, the fiber density was 63.7 ± 7.4 % while the corresponding value was 66.9 ± 5.8 % in the inner zone. Fiber density decreased slightly with increasing total Pauli score [Fig. 7(a)]. Linear regression showed a decrease (95 % CI) of -1.4 $(-2.4, -0.34)$ percentage points per score in the inner zone. The decrease was not statistically significant in the middle zone with -0.38 $(-1.9, 1.1)$ percentage points per score.

Fiber orientation

Orientation maps calculated from the structure tensor allow to clearly visualize the fiber directions (Fig. 4). In the orientation analysis, one VOI (same as for the fiber density), was excluded from the analysis. FAHM from the orientation maps was 7.8 ± 5.1 % (mean
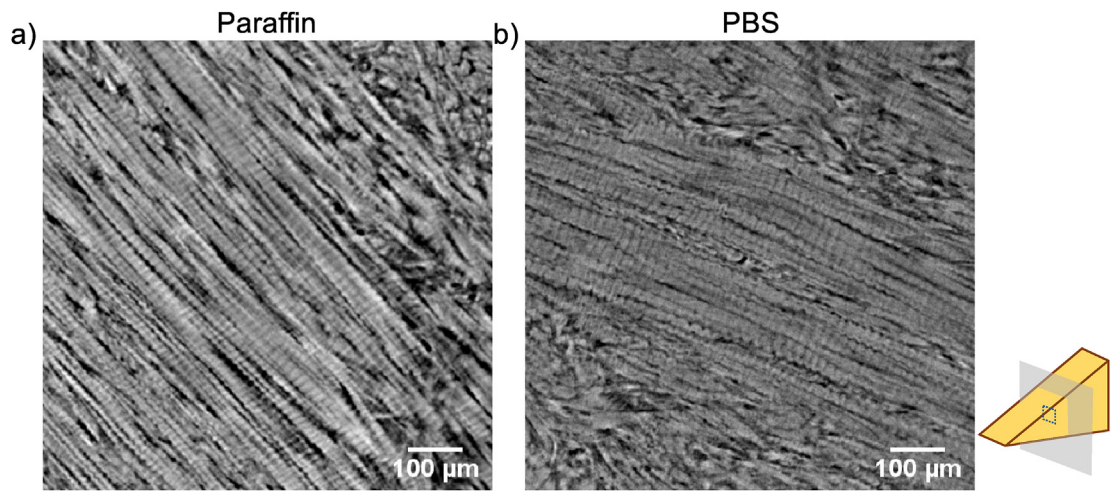
Fig. 2

Osteoarthritis and Cartilage

Example images showing sagittal cross-sections (as shown in the schematics) of two samples from the same meniscus that undergone different types of preparation, (a) imaged fixed and embedded in paraffin, and (b) frozen and thawed in PBS.
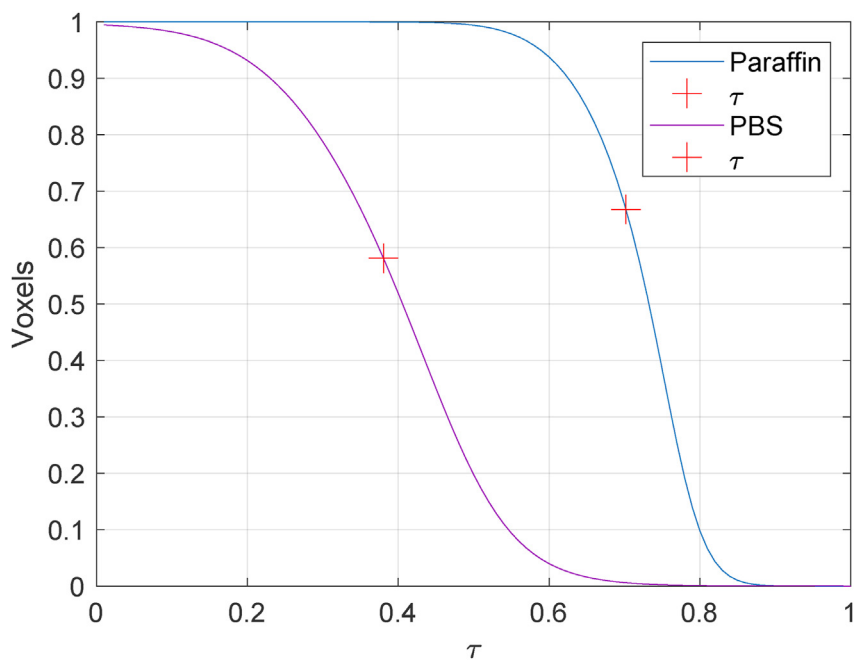

Fig. 3

Osteoarthritis and Cartilage

Proportion of image voxels categorized as fibers, plotted against grayscale threshold value τ for a fresh frozen sample in PBS (purple line) and a fixed paraffin embedded sample (blue line) from the same meniscus. τ calculated using Otsu's method is marked with a red cross for each sample. The slope is steeper for the paraffin-embedded sample which indicates a larger contrast between fiber and background voxels in comparison to the sample in PBS. However, Otsu's method still results in similar number of voxels categorized as fibers and background.
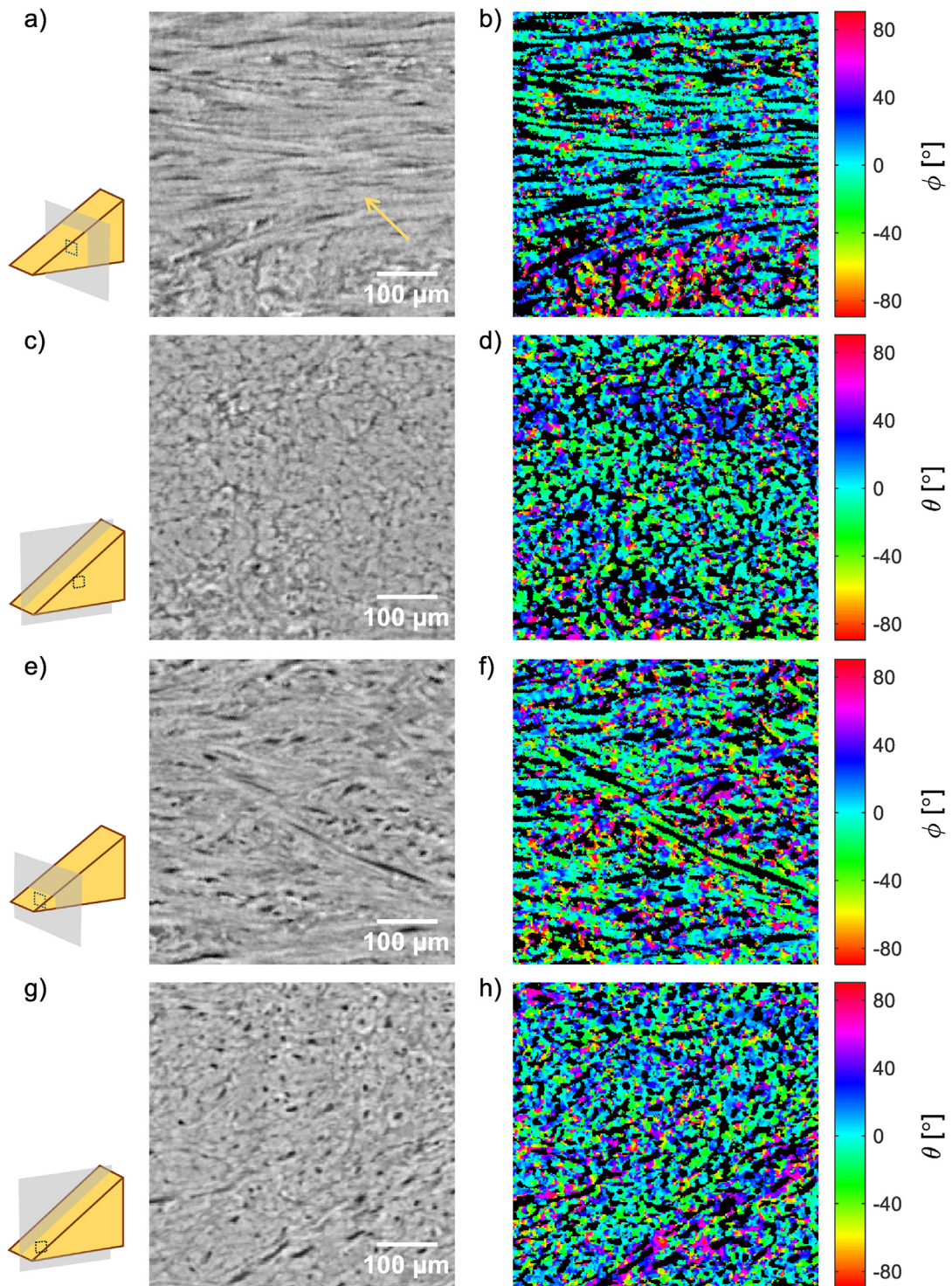
Fig. 4

(a) Example of a grayscale sagittal image where circumferential fiber bundles (arrow) are seen oriented horizontally within this image plane. In (b) the corresponding azimuth angle (φ) orientation map, this is seen as mostly turquoise (i.e., azimuthal angles close to 0). (c) A coronal slice of the same image volume, fibers are directed mainly through the image plane with elevation angles also close to 0 which is seen in (d) the elevation angle (θ) orientation map. (e-h) display corresponding images and orientation maps from the inner zone of the same meniscus where the fibers can be seen to deviate more from the horizontal direction.
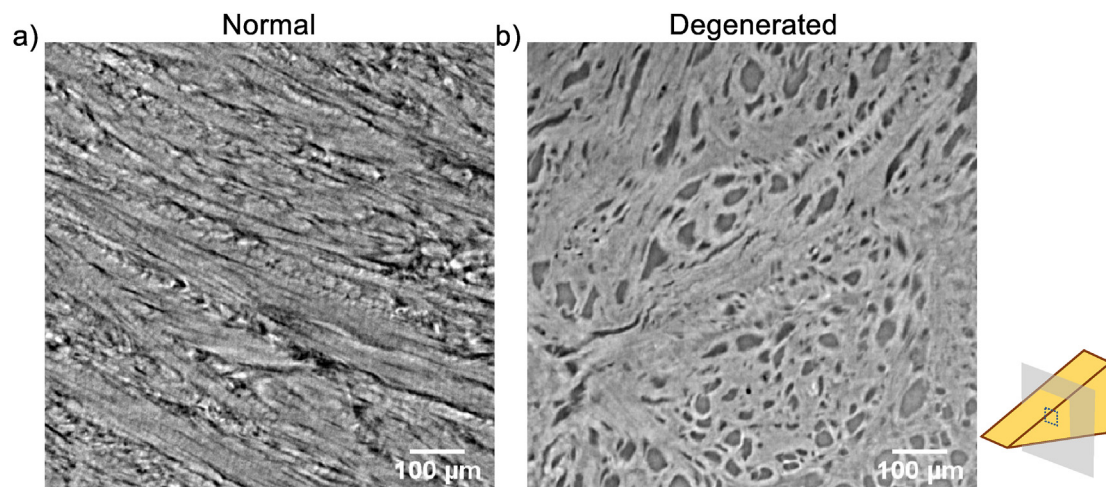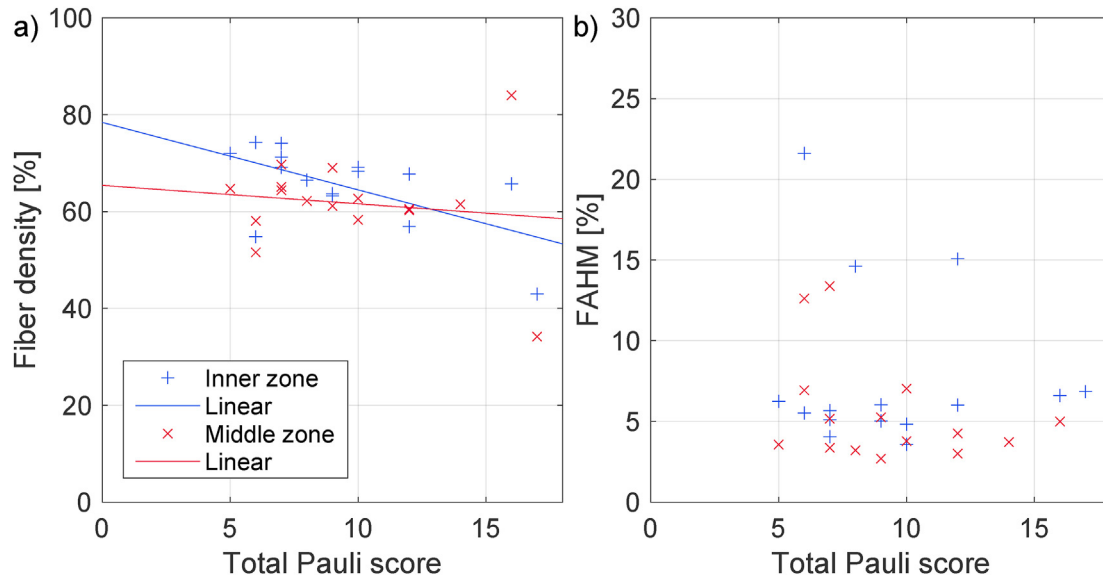
Fig. 5 | Osteoarthritis and Cartilage

Example images of the inner zone, close to the surface, of (a) a normal meniscus (Pauli score 6) and (b) a degenerated meniscus (Pauli score 16).
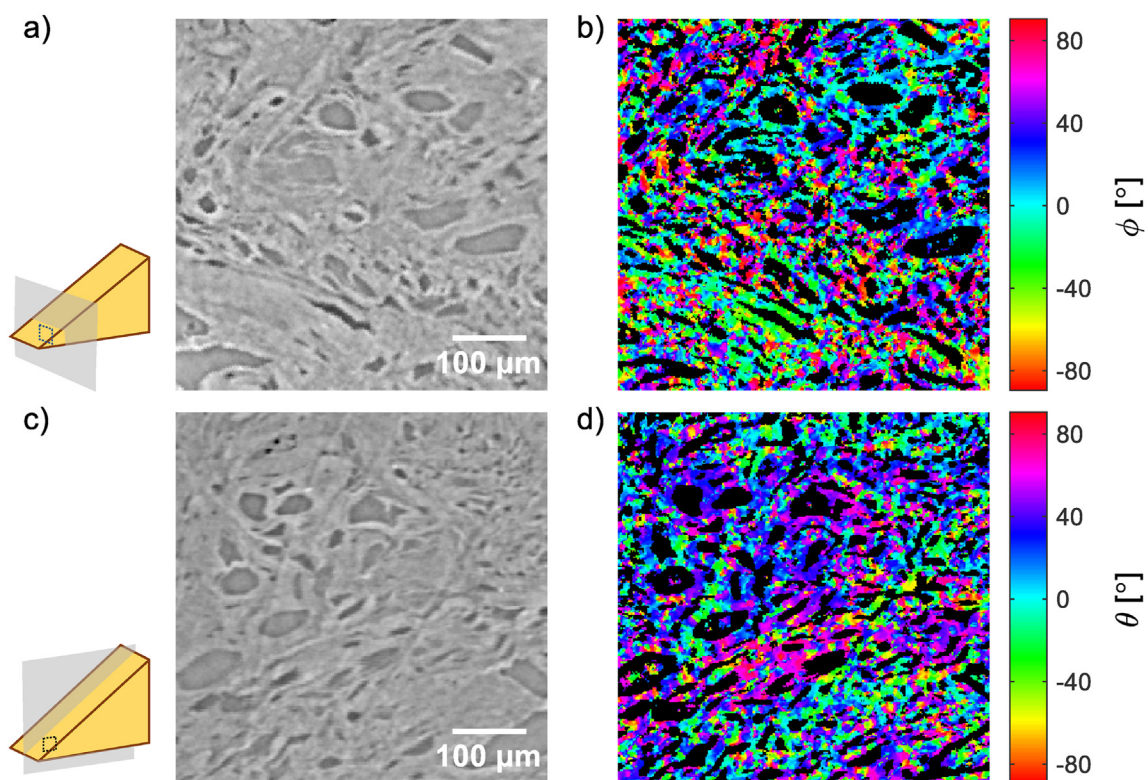
Fig. 6 | Osteoarthritis and Cartilage

Example images in (a) a sagittal and (c) coronal plane with corresponding orientation maps of (b) azimuth (φ) and (d) elevation (θ) angle from the inner zone of a degenerated meniscus (Pauli score 16).

Fig. 7

Osteoarthritis and Cartilage

(a) Fiber density, presented as a function of total Pauli score, in the inner and middle zone of each of the fresh frozen samples, respectively (n = 16). The inner zone of one sample was excluded due to severe degeneration. (b) FAHM in percentage of bins from the 2D histogram over azimuth and elevation angles, presented as a function of total Pauli score for the VOI in the inner and middle zone, respectively, for each of the fresh frozen samples except the inner zone of one sample (same as in a) and the middle zone of another sample (outlier).

and standard deviation) in the inner zone and 8.7 ± 3.3 % in the middle zone, excluding one value that was an outlier (FAHM of 56 %). Comparison with Pauli score did not appear to show any clear association [Fig. 7(b)]. This was also confirmed in the statistical analysis where the difference in FAHM per Pauli score (95 % CI) was −13.9 (−93.6, 65.8) % in the inner zone and −35.8 (−90.5, 18.8) % in the middle zone.

Fiber crimping period

The fiber crimping patterns were clearly seen in most of the samples (see for example the wavy appearance of the fibers in Fig. 2) and were observed mainly in the middle zone and sparser and sparser closer to the inner tip. Crimping period was measured in the middle zone of all samples except one (total Pauli score of 17) where no crimped fibers were observed. The mean crimping period was 23.8 ± 3.1 μm. No clear association was seen with Pauli score (Fig. 8). Difference in crimping period per score (95 % CI) was 0.23 (−0.25, 0.70) μm.

Discussion

In this study we have presented images of human meniscus tissue obtained with the promising SR-PhC-μCT technique. Most importantly, high-resolution images were obtained in 3D where collagen microstructure, including crimping morphology, was clearly visualized without the use of tissue fixation or embedding.

Image quality was similar for the thawed fresh frozen samples in PBS and samples that were fixed and embedded in paraffin. Images of the paraffin embedded samples showed a slightly improved contrast and a very distinct crimping pattern, which could be an effect of the fixation process, as it can result in shrinkage of the fibers[30,31]. Fresh frozen, non-fixed samples on the other hand have

gone through fewer critical tissue-processing steps and are closer to the native tissue.

The number of voxels defined as fibers were similar between the inner and the middle zone, but fewer crimped fibers were seen in the inner zone. This is in agreement with earlier studies showing collagen of the inner zone to be more similar to that of articular cartilage compared to the rest of the meniscus[32,33]. In general, it appeared that FAHM might be higher in the inner zone compared to the middle zone. We hypothesized that the calculated FAHM of the azimuth and elevation angles from the structure tensor would reflect tissue degeneration as described by Pauli score. With the current limited set of samples, we could however not observe such an association. Both vertical and horizontal slices are needed for the histopathological evaluation with the Pauli scoring system. The organization of collagen fibers was evaluated in the horizontal slices that were cut from a location in the posterior horn, further away from the samples imaged using SR-PhC-μCT compared to the vertical histology slices. Local variation in degenerative state within the meniscus could thus contribute to the weak association of total Pauli score and FAHM from the orientation analysis. We chose to use FAHM as a measure of angular spread to eliminate difference in sample orientation that is of importance to absolute fiber angles. To evaluate the absolute angles, reference axes would need to be established that relates the fiber angle to the macroscopic orientation of the sample.

We expected degeneration to have an effect mainly on the distribution of orientations of collagen fibers and maybe not as much on the collagen fiber density since mainly disruption and disorganization of the collagen network has been reported as a sign of meniscus degeneration[7,8]. The larger cavities that we observed in the most degenerated samples suggest however that there is also a loss of collagen architecture. This was observed most clearly near
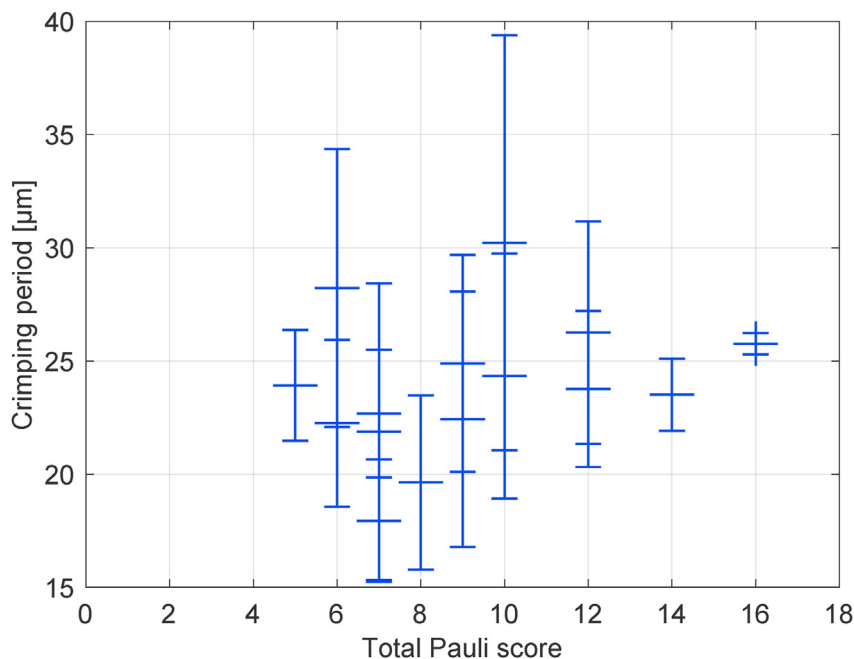
Fig. 8

Osteoarthritis and Cartilage

Crimping period averaged over five locations for each of the fresh frozen meniscus samples, presented as a function of total Pauli score. Error bars represent standard deviation among the five values.

the surface of the meniscus sample, which could be the reason it was not reflected in the quantified fiber density that was calculated at the center of the sample. Also, parameters of the image analysis, e.g., suitable levels of filtering, was set based on generally intact samples. It was observed that voxels within the cavities in severely degenerated areas were sometimes misinterpreted as fibers. The image analysis may therefore not be accurate in such visibly degenerated areas of the tissue samples and is thus not included in this work.

Although the meniscus is a highly structured tissue, there is still a larger native spread in fiber orientation compared to the Achilles tendon, where this orientation analysis has been successfully applied before[16]. This probably makes sample orientation more critical and interpretation of the results more difficult in meniscus samples compared to tendons.

Values of crimping period in the present study are of about the same magnitude as reported earlier[18,19]. Michalek et al., reported values of crimp period in the lamellar layer of deer menisci of around 20—30 µm in healthy controls and around 10 µm in enzymatically degraded samples[18]. Values of crimping length, equaling half the period, of 3.7—9.4 µm was reported in human meniscal attachments by Villegas et al.[19]. The variation could relate to differences in the location tested or between species as well as the difference in techniques. In these earlier studies, crimping was measured in images obtained by PLM and SEM (thus in 2D and after substantial sample preparation), whereas our study shows that this can be done also in 3D image data sets from SR-PhC-µCT imaging of fresh frozen tissue.

Crimping morphology has been studied in relation to mechanical loading for example by snap-freezing of tissue samples during loading[34,35]. Attempts has been done to integrate PLM with a mechanical testing devise for imaging of tendon[36]. Similar studies of the tissue structure response to mechanical loading could also be of interest in menisci. For such future studies it would be preferable to be able to image samples without fixation and embedding since imaging and loading then could be performed using the same set-up. Preparation of tissue using fixation fluid and contrast agents might also affect the structure of the tissue[10]. Our results show that the image quality in fresh frozen samples is sufficient to distinguish structural features such as individual fibers and fiber crimping. Thus, experiments of meniscus biomechanics may be possible in tissue that is closer to its natural state using SR-PhC-µCT.

In this study, we used frozen samples that were thawed before imaging. Freezing has a potential effect on the tissue with destruction of cells and possible alteration of the collagen network as the result[37,38]. The freezing was however necessary due to the longitudinal storage of samples in our biobank, and to the long distance to the synchrotron light source used. Access to the light source is limited and needs to be planned in advance which makes studies using fresh (never frozen) samples extremely challenging. Cryopreservation has been reported to have less impact on the tissue and might be an alternative preservation method for samples in future studies[39].

The calculation of crimping period, as implemented here, was dependent on manually drawn image profiles. How clear the crimps were seen varied between locations and samples and the subjective choice of profile position within the sample may have influenced the power spectrum. Also, the selection of the peak corresponding to the crimping was not always obvious since some spectra had more than one peak (Supplementary Fig. S3). Ring

artifacts that were seen in several of the samples may have contributed to the appearance of the power spectra. In future studies, it would be desired to further develop the analysis to be more automatized and to utilize the full 3D nature of the dataset.

Although crimping is a tissue property of great interest, it should be considered that the crimping pattern may affect the orientation analysis since it can be interpreted as a variation in fiber orientation. In our analysis this effect may have influenced the evaluation of fiber orientations when calculating the FAHM. We evaluated the effect of different filtering approaches, but none could fully smooth out the crimping pattern without inducing other artefacts.

Evaluation of the suggested image analysis parameters were limited by the small sample size and the lack of tissue samples with confirmed disease. Future studies would benefit from an increased samples size, preferably also including samples from persons with confirmed knee OA. Further work is also needed to establish parameters that can be used as reliable quantitative or semi-quantitative measures of image structure to describe tissue quality and/or function.

In conclusion, it is feasible to acquire SR-PhC-μCT images of human meniscus tissue samples with sufficient spatial resolution to visualize the collagen fiber structure and crimping morphology without the use of tissue fixation or embedding. Further studies are needed to establish and validate quantitative image-based measures of tissue degeneration. SR-PhC-μCT could then become a useful tool in future studies of meniscus biomechanics and tissue degeneration.

Contributions

EE: Study design, sample preparation, image analysis, interpretation of data, drafting the manuscript. MP: Study design, sample preparation, image acquisition and reconstruction, image analysis, interpretation of data, revising the manuscript. VN: Image acquisition and reconstruction, revising the manuscript. JS: Study design, interpretation of data, revising the manuscript. HI: Study design, image acquisition and reconstruction, interpretation of data, revising the manuscript. ME: Study design, sample preparation, image acquisition, interpretation of data, revising the manuscript. Professor M. Englund (martin.englund@med.lu.se) takes responsibility for the integrity of this work as a whole.

Conflict of interest
The authors have no competing interests to declare.

Supplementary data

Supplementary data to this article can be found online at https://doi.org/10.1016/j.joca.2022.06.003.

References

1. Englund M, Guermazi A, Roemer FW, Aliabadi P, Yang M, Lewis CE, *et al.* Meniscal tear in knees without surgery and the development of radiographic osteoarthritis among middle-aged and elderly persons: the multicenter osteoarthritis study. Arthritis Rheum 2009;60(3):831–9, https://doi.org/10.1002/art.24383. Epub 2009/02/28. PubMed PMID: 19248082; PubMed Central PMCID: PMC2758243.
2. Petersen W, Tillmann B. Collagenous fibril texture of the human knee joint menisci. Anat Embryol 1998;197(4):317–24, https://doi.org/10.1007/s004290050141. Epub 1998/06/13. PubMed PMID: 9565324.
3. Aspden RM, Yarker YE, Hukins DW. Collagen orientations in the meniscus of the knee joint. J Anat 1985;140(Pt 3):371–80. Epub 1985/05/01. PubMed PMID: 4066476; PubMed Central PMCID: PMC1165103.
4. Gathercole LJ, Keller A. Crimp morphology in the fibre-forming collagens. Matrix 1991;11(3):214–34, https://doi.org/10.1016/s0934-8832(11)80161-7. Epub 1991/06/01. PubMed PMID: 1870453.
5. Franchi M, Trirè A, Quaranta M, Orsini E, Ottani V. Collagen structure of tendon relates to function. Sci World J 2007;7:404–20, https://doi.org/10.1100/tsw.2007.92. Epub 2007/04/24. PubMed PMID: 17450305; PubMed Central PMCID: PMC5901217.
6. Wren TA, Carter DR. A microstructural model for the tensile constitutive and failure behavior of soft skeletal connective tissues. J Biomech Eng 1998;120(1):55–61, https://doi.org/10.1115/1.2834307. Epub 1998/07/24. PubMed PMID: 9675681.
7. Pauli C, Grogan SP, Patil S, Otsuki S, Hasegawa A, Koziol J, *et al.* Macroscopic and histopathologic analysis of human knee menisci in aging and osteoarthritis. Osteoarthritis Cartilage 2011;19(9):1132–41, https://doi.org/10.1016/j.joca.2011.05.008. Epub 2011/06/21. PubMed PMID: 21683797; PubMed Central PMCID: PMC3217905.
8. Herwig J, Egner E, Buddecke E. Chemical changes of human knee joint menisci in various stages of degeneration. Ann Rheum Dis 1984;43(4):635–40. Epub 1984/08/01. PubMed PMID: 6548109; PubMed Central PMCID: PMC1001426.
9. Horng A, Brun E, Mittone A, Gasilov S, Weber L, Geith T, *et al.* Cartilage and soft tissue imaging using X-rays: propagation-based phase-contrast computed tomography of the human knee in comparison with clinical imaging techniques and histology. Invest Radiol 2014;49(9):627–34, https://doi.org/10.1097/rli.0000000000000063. Epub 2014/05/16. PubMed PMID: 24825531.
10. Disney CM, Madi K, Bodey AJ, Lee PD, Hoyland JA, Sherratt MJ. Visualising the 3D microstructure of stained and native intervertebral discs using X-ray microtomography. Sci Rep 2017;7(1), 16279, https://doi.org/10.1038/s41598-017-16354-w. Epub 2017/11/28. PubMed PMID: 29176563; PubMed Central PMCID: PMC5701246.
11. Horng A, Stroebel J, Geith T, Milz S, Pacureanu A, Yang Y, *et al.* Multiscale X-ray phase contrast imaging of human cartilage

for investigating osteoarthritis formation. J Biomed Sci 2021;28(1):42, https://doi.org/10.1186/s12929-021-00739-1. Epub 2021/06/09. PubMed PMID: 34098949; PubMed Central PMCID: PMC8182937.

12. Betz O, Wegst U, Weide D, Heethoff M, Helfen L, Lee WK, *et al.* Imaging applications of synchrotron X-ray phase-contrast microtomography in biological morphology and biomaterials science. I. General aspects of the technique and its advantages in the analysis of millimetre-sized arthropod structure. J Microsc 2007;227(Pt 1):51–71, https://doi.org/10.1111/j.1365-2818.2007.01785.x. Epub 2007/07/20. PubMed PMID: 17635659.

13. Pierantoni M, Silva Barreto I, Hammerman M, Verhoeven L, Törnquist E, Novak V, *et al.* A quality optimization approach to image Achilles tendon microstructure by phase-contrast enhanced synchrotron micro-tomography. Sci Rep 2021;11(1), 17313, https://doi.org/10.1038/s41598-021-96589-w. Epub 2021/08/29. PubMed PMID: 34453067; PubMed Central PMCID: PMC8397765.

14. Krause M, Hausherr JM, Burgeth B, Herrmann C, Krenkel W. Determination of the fibre orientation in composites using the structure tensor and local X-ray transform. J Mater Sci 2010;45(4):888–96, https://doi.org/10.1007/s10853-009-4016-4.

15. Straumit I, Lomov Stephan V, Wevers Martine. Quantification of the internal structure and automatic generation of voxel models of textile composites from X-ray computed tomography data. Compos Appl Sci Manuf 2015;69:150–8, https://doi.org/10.1016/j.compositesa.2014.11.016. Epub 2014/11/15.

16. Pierantoni M, Silva Baretto I, Hammerman M, Törnquist E, Novak V, Eliasson P, Isaksson H. Can synchrotron phase contrast micro-tomography uncover how in vivo loading affects the Achilles tendon structure?. Stockholm: XXVIII Congress of the International Society of Biomechanics (ISB); 2021.

17. Karjalainen VP, Kestilä I, Finnilä MA, Folkesson E, Turkiewicz A, Önnerfjord P, *et al.* Quantitative three-dimensional collagen orientation analysis of human meniscus posterior horn in health and osteoarthritis using micro-computed tomography. Osteoarthritis Cartilage 2021;29(5):762–72, https://doi.org/10.1016/j.joca.2021.01.009. Epub 2021/02/16. PubMed PMID: 33588085; PubMed Central PMCID: PMC7610734.

18. Michalek AJ, Kuxhaus L, Jaremczuk D, Zaino NL. Proteoglycans contribute locally to swelling, but globally to compressive mechanics, in intact cervine medial meniscus. J Biomech 2018;74:86–91, https://doi.org/10.1016/j.jbiomech.2018.04.023. Epub 2018/05/01. PubMed PMID: 29705348.

19. Villegas DF, Donahue TL. Collagen morphology in human meniscal attachments: a SEM study. Connect Tissue Res 2010;51(5):327–36, https://doi.org/10.3109/03008200903349639. Epub 2010/04/15. PubMed PMID: 20388017.

20. Villegas DF, Hansen TA, Liu DF, Donahue TL. A quantitative study of the microstructure and biochemistry of the medial meniscal horn attachments. Ann Biomed Eng 2008;36(1):123–31, https://doi.org/10.1007/s10439-007-9403-x. Epub 2007/11/14. PubMed PMID: 17999192.

21. Kestilä I, Folkesson E, Finnilä MA, Turkiewicz A, Önnerfjord P, Hughes V, *et al.* Three-dimensional microstructure of human meniscus posterior horn in health and osteoarthritis. Osteoarthritis Cartilage 2019;27(12):1790–9, https://doi.org/10.1016/j.joca.2019.07.003. Epub 20190710. PubMed PMID: 31301431; PubMed Central PMCID: PMC7610688.

22. Stampanoni M, Groso A, Isenegger A, Mikuljan G, Chen Q, Bertrand A, *et al.* Trends in Synchrotron-Based Tomographic Imaging: The SLS Experience. SPIE; 2006.

23. Paganin D, Mayo SC, Gureyev TE, Miller PR, Wilkins SW. Simultaneous phase and amplitude extraction from a single defocused image of a homogeneous object. J Microsc 2002;206(Pt 1):33–40, https://doi.org/10.1046/j.1365-2818.2002.01010.x. Epub 2002/05/10. PubMed PMID: 12000561.

24. Marone F, Stampanoni M. Regridding reconstruction algorithm for real-time tomographic imaging. J Synchrotron Radiat 2012;19(Pt 6):1029–37, https://doi.org/10.1107/s0909049512032864. Epub 2012/10/25. PubMed PMID: 23093766; PubMed Central PMCID: PMC3480277.

25. Modregger P, Lübbert D, Schäfer P, Köhler R. Spatial resolution in Bragg-magnified X-ray images as determined by Fourier analysis. Phys Status Solidi 2007;204(8):2746–52, https://doi.org/10.1002/pssa.200675685.

26. Lovric G, Barré SF, Schittny JC, Roth-Kleiner M, Stampanoni M, Mokso R. Dose optimization approach to fast X-ray micro-tomography of the lung alveoli. J Appl Crystallogr 2013;46(Pt 4):856–60, https://doi.org/10.1107/s0021889813005591. Epub 2013/09/21. PubMed PMID: 24046488; PubMed Central PMCID: PMC3769076.

27. Yester M, Barnes G. Geometrical Limitations of Computed Tomography (CT) Scanner Resolution. SPIE; 1977.

28. Otsu N. A threshold selection method from gray-level histograms. IEEE Trans Syst Man Cybernet 1979;9(1):62–6, https://doi.org/10.1109/TSMC.1979.4310076.

29. Mulat C, Donias M, Baylou P, Vignoles G, Germain C. Axis detection of cylindrical objects in three-dimensional images. J Electron Imag 2008;17(3), 031108.

30. Dias CSB, Neto DPA, Baraldi GL, Fonseca MC. Comparative analysis of sample preparation protocols of soft biological tissues for morphometric studies using synchrotron-based X-ray microtomography. J Synchrotron Radiat 2019;26(Pt 6):2013–23, https://doi.org/10.1107/s1600577519011299. Epub 2019/11/14. PubMed PMID: 31721746.

31. Zehbe R, Haibel A, Riesemeier H, Gross U, Kirkpatrick CJ, Schubert H, *et al.* Going beyond histology. Synchrotron micro-computed tomography as a methodology for biological tissue characterization: from tissue morphology to individual cells. J R Soc Interface 2010;7(42):49–59, https://doi.org/10.1098/rsif.2008.0539. Epub 2009/03/28. PubMed PMID: 19324670; PubMed Central PMCID: PMC2839371.

32. Cheung HS. Distribution of type I, II, III and V in the pepsin solubilized collagens in bovine menisci. Connect Tissue Res 1987;16(4):343–56, https://doi.org/10.3109/03008208709005619. Epub 1987/01/01. PubMed PMID: 3132349.

33. Folkesson E, Turkiewicz A, Rydén M, Hughes HV, Ali N, Tjörnstrand J, *et al.* Proteomic characterization of the normal human medial meniscus body using data-independent acquisition mass spectrometry. J Orthop Res 2020;38(8):1735–45, https://doi.org/10.1002/jor.24602. Epub 2020/01/29. PubMed PMID: 31989678; PubMed Central PMCID: PMC7610686.

34. Miller KS, Connizzo BK, Feeney E, Soslowsky LJ. Characterizing local collagen fiber re-alignment and crimp behavior throughout mechanical testing in a mature mouse supraspinatus tendon model. J Biomech 2012;45(12):2061–5, https://doi.org/10.1016/j.jbiomech.2012.06.006. Epub 2012/07/11. PubMed PMID: 22776688; PubMed Central PMCID: PMC3405169.

35. Kääb MJ, Ito K, Clark JM, Nötzli HP. The acute structural changes of loaded articular cartilage following meniscectomy or ACL-transection. Osteoarthritis Cartilage 2000;8(6):464–73, https://doi.org/10.1053/joca.1999.0322. Epub 2000/11/09. PubMed PMID: 11069731.

36. Zuskov A, Freedman BR, Gordon JA, Sarver JJ, Buckley MR, Soslowsky LJ. Tendon biomechanics and crimp properties following fatigue loading are influenced by tendon type and age in mice. J Orthop Res 2020;38(1):36–42, https://doi.org/10.1002/jor.24407. Epub 2019/07/10. PubMed PMID: 31286548; PubMed Central PMCID: PMC6917867.

37. Gelber PE, Gonzalez G, Lloreta JL, Reina F, Caceres E, Monllau JC. Freezing causes changes in the meniscus collagen net: a new ultrastructural meniscus disarray scale. Knee Surg Sports Traumatol Arthrosc 2008;16(4):353–9, https://doi.org/10.1007/s00167-007-0457-y. Epub 2007/12/11. PubMed PMID: 18066525.

38. Salai M, Givon U, Messer Y, von Versen R. Electron microscopic study on the effects of different preservation methods for meniscal cartilage. Ann Transplant 1997;2(1):52–4. Epub 1997/01/01. PubMed PMID: 9869843.

39. Jacquet C, Erivan R, Sharma A, Pithioux M, Parratte S, Argenson JN, et al. Preservation methods influence the biomechanical properties of human lateral menisci: an ex vivo comparative study of 3 methods. Orthop J Sports Med 2019;7(4), 2325967119841622, https://doi.org/10.1177/2325967119841622. Epub 2019/05/09. PubMed PMID: 31065555; PubMed Central PMCID: PMC6488788.